Structural Dynamics of Ligand Diffusion in the Protein Matrix: A Study on a New Myoglobin Mutant Y(B10) Q(E7) R(E10)

M. Brunori,* F. Cutruzzolà,* C. Savino,* C. Travaglini-Allocatelli,* B. Vallone,* and Q. H. Gibson#
*Department of Biochemical Sciences and CNR Center of Molecular Biology, University of Rome "La Sapienza," Rome, Italy, and #Department of Biochemistry and Cell Biology, Rice University, Houston, Texas, USA

ABSTRACT A triple mutant of sperm whale myoglobin (Mb) [Leu(B10) → Tyr, His(E7) → Gln, and Thr(E10) → Arg, called Mb-YQR], investigated by stopped-flow, laser photolysis, crystallography, and molecular dynamics (MD) simulations, proved to be quite unusual. Rebinding of photodissociated NO, O_2, and CO from within the protein (in a "geminate" mode) allows us to reach general conclusions about dynamics and cavities in proteins. The 3D structure of oxy Mb-YQR shows that bound O_2 makes two H-bonds with Tyr(B10)29 and Gln(E7)64; on deoxygenation, these two residues move toward the space occupied by O_2. The bimolecular rate constant for NO binding is the same as for wild-type, but those for CO and O_2 binding are reduced 10-fold. While there is no geminate recombination with O_2 and CO, geminate rebinding of NO displays an unusually large and very slow component, which is pretty much abolished in the presence of xenon. These results and MD simulations suggest that the ligand migrates in the protein matrix to a major "secondary site," located beneath Tyr(B10)29 and accessible via the motion of Ile(G8)107; this site is different from the "primary site" identified by others who investigated the photolyzed state of wild-type Mb by crystallography. Our hypothesis may rationalize the O_2 binding properties of Mb-YQR, and more generally to propose a mechanism of control of ligand binding and dissociation in hemeproteins based on the dynamics of side chains that may (or may not) allow access to and direct temporary sequestration of the dissociated ligand in a docking site within the protein. This interpretation suggests that very fast (picosecond) fluctuations of amino acid side chains may play a crucial role in controlling O_2 delivery to tissue at a rate compatible with physiology.

INTRODUCTION

Myoglobin (Mb) has been widely used as a prototype macromolecule for investigating structural dynamics of ligand binding and protein relaxation phenomena. Following the classical work of Austin et al. (1975), studies on the reaction of Mb with CO and other ligands have revealed the role of conformational substates, which were identified and characterized by laser photolysis experiments at different temperatures, using wild-type and mutant Mbs (Frauenfelder et al., 1990; Hofrichter et al., 1983; Gibson, 1989; Huang and Boxer, 1994; Olson and Phillips, 1996). A docking site for the photodissociated CO in the distal pocket of Mb has been identified by x-ray diffraction studies in single crystals either at ultra-low temperatures (Schlichting et al., 1994; Teng et al., 1994) or at room temperature with nanosecond time resolution (Srajer et al., 1996). These pioneering investigations have shown that in the photolyzed state, the CO has drifted away from the iron, which (partially) moves out of the mean heme plane. The ligand lies in a definite orientation in the heme pocket, on top of heme's pyrrole ring C and confined by residues Leu(B10)29, Phe(CD1)43, His(E7)64, Val(E11)68, and Ile(G8)107. Protein relaxations after photolysis were also detected and compared with data from transient spectroscopy and molecular dynamics (MD) simulations.

Received for publication 27 July 1998 and in final form 24 November 1998.
Address reprint requests to M. Brunori, Dipartimento di Scienze Biochimiche, Università "La Sapienza," P.le Aldo Moro 5, 00185 Roma, Italy. Tel.: 39-06-4450291; Fax: 39-06-4440062; E-mail: brunori@axrma.uniroma1.it.

0006-3495/99/03/1259/11 $2.00

The rebinding of ligands to Mb after laser photolysis has been classically described by one first-order and one second-order reaction according to the scheme discussed by Olson and Phillips (1996), involving two barriers and three states:

$$\mathrm{MbL} \Leftrightarrow \mathrm{Mb} \cdots \mathrm{L} \Leftrightarrow \mathrm{Mb} + \mathrm{L} \qquad (1)$$

The kinetics of wild-type and mutant Mbs after laser photolysis of CO, O_2, NO, and the isocyanides, analyzed according to Scheme 1, yielded essential findings concerning the specific role of amino acid side chains in the distal pocket in controlling geminate rebinding, ligand escape to the bulk, and thus overall rates and affinities (Springer et al., 1994; Olson and Phillips, 1996). Experiments with higher resolution (Chatfield et al., 1990) required, however, two first-order parameters to describe nanosecond rebinding of O_2; this was confirmed by Scott and Gibson (1997) in experiments with sperm whale Mb mutants, in which the effect of high pressure of xenon on recombination kinetics was examined. These data were interpreted with a branched kinetic scheme which proposed that, in addition to the "primary site" in the distal pocket (see above), a "secondary site" within the protein matrix may transiently host the photodissociated ligand. These results were in support of previous work by Huang and Boxer (1994) who showed (by random mutagenesis of Mb and laser photolysis) that ligand escape after photodissociation can occur via different possible pathways through the protein.

In the present work a conceptually similar approach is applied to a triple mutant of sperm whale Mb, initially designed to mimic the distal pocket of *Ascaris suum* hemo-

globin (Hb) (De Baere et al., 1994; Yang et al., 1995). The latter protein is very peculiar because of its extremely low O_2 dissociation rate constant ($K = 0.004\ s^{-1}$) (Davenport, 1949), which was attributed to additional H-bonding power of a Tyr residue in the pocket, at topological position (B10) (De Baere et al., 1994). More recent work by Peterson et al. (1997) indicated that the peculiar O_2 affinity of *Ascaris* Hb may demand large amplitude fluctuations, which couple the loss of distal H-bonding to the opening of a tight distal cage. The triple mutant of sperm whale Mb we synthesized (called Mb-YQR) (Travaglini-Allocatelli et al., 1994) has the following substitutions: Leu(B10) → Tyr, His(E7) → Gln, Thr(E10) → Arg. Its O_2 affinity constant is $1.2 \times 10^6\ M^{-1}$ compared to $0.9 \times 10^6\ M^{-1}$ for wt Mb; however, this value arises from a different set of combination and dissociation rate constants, namely a lowered combination rate ($2 \times 10^6\ M^{-1}\ s^{-1}$ vs. $1.5 \times 10^7\ M^{-1}\ s^{-1}$) and an almost equally lowered dissociation rate ($1\ s^{-1}$ vs. $14\ s^{-1}$) (Travaglini-Allocatelli et al., 1994). As shown below, this result is consistent with additional H-bonding to O_2 provided by distal side chains, as identified from the high-resolution 3D structure of oxy Mb-YQR. Bound O_2 has a different orientation compared to the "standard" geometry, and establishes one H-bond with the hydroxyl group of Tyr(B10)29 and another with Gln(E7)64. Interestingly, Tyr(B10)29 and Gln(E7)64 have the same orientation seen in *Ascaris* Hb and the same distances from bound O_2 (Yang et al., 1995); however, the orientation of the imidazole ring of the proximal His relative to the heme axis is different in the two proteins. The 3D structure of deoxy Mb-YQR shows that Tyr(B10)29 and Gln(E7)64 move on deoxygenation, which may account for the observed decrease in the association rate constants.

The high resolution structure of oxy and deoxy Mb-YQR cannot explain, however, why the dissociation rate constant of this triple mutant is still >200-fold faster than that of *Ascaris* Hb. Therefore, we resorted to an experimental investigation of structural dynamics by laser-activated geminate kinetics of O_2, NO, and CO, as well as MD simulations. The data indicate that the unique properties of Mb-YQR may be interpreted by a branched mechanism, implying an accessible "secondary site" within the protein matrix, following the model discussed by Scott and Gibson (1997). This site, which has been identified by MD simulations and confirmed by the effect of xenon on the geminate kinetics, is clearly distinct from the "primary site" identified in the photolyzed state of wild-type Mb (Schlichting et al., 1994; Teng et al., 1994), being beneath Tyr(B10)29. Interestingly, it is made accessible in Mb-YQR mutant by picosecond fluctuations of Ile(G8)107, while it is not accessible in *Ascaris* Hb because a Phe at position G8 blocks the channel. The general lesson emerging from this work is the necessity to explore protein motions over a very wide dynamic range in order to achieve a molecular rationale for overall, biochemically relevant, functional parameters.

MATERIALS AND METHODS

Biochemistry

Mutant Mb-YQR was expressed in *Escherichia coli* and the protein purified as described before (Travaglini-Allocatelli et al., 1994). The optical spectra of the different derivatives of Mb-YQR (including the NO complex) are very similar or identical to wt Mb. Crystals were grown at 21°C using the vapor diffusion technique, as described by Phillips et al. (1990), by mixing 5 μl of 1 mM protein solution with an equal volume of 2.7 M ammonium sulfate solution in 20 mM Tris-Cl at pH 8.7 and 1 mM EDTA, and equilibrated with the same solution. Crystals grow in approximately two weeks and belong to the hexagonal group P6 (for details on cell dimensions and data collection, see Table 1).

Crystallography

Deoxy Mb-YQR crystals were obtained by the addition of 10 mM sodium dithionite; a clear change in color, consistent with deoxygenation, was observed during soaking. The deoxy crystal was mounted in a capillary under anaerobic conditions. To obtain the oxygenated derivative, the crystal after reduction was washed three times with the mother liquor equilibrated in air, and after several hours the color changed to bright red, showing oxygenation; at this point after soaking in mother liquor containing 20% glycerol, the crystal was frozen at 120 K for data collection. During soaking with the cryoprotectant, the crystal spontaneously broke into two; we exposed one of the two to the x-rays and took an optical spectrum of the other, which showed that Mb-YQR was completely oxygenated. The same spectral analysis was performed on the crystal exposed to x-rays after data collection.

Diffraction data were collected using a Rigaku R-Axis II (Tokyo, Japan) image plate system mounted on a copper rotating anode generator and focused by a mirror system; 1.5° oscillation images were collected and the data were processed using DENZO (Otwinowsky and Minor, 1996). All subsequent data handling was carried out using the CCP4 package (Collaborative Computional Project Number 4, 1994). Both the oxy and deoxy derivatives diffracted to a resolution better than 2 Å; other details on data collection are given in Table 1. Refinement was carried out using the structure of wild-type sperm whale Mb expressed by *E. coli* (PDB code 2 mg; Phillips et al., 1990). The initial R-factor was 26% for the deoxy derivative and 40% for the oxy derivative, consistent with the slight shrinking of the cell upon freezing. Refinement was performed using the maximum likelihood program REFMAC (Murshdov et al., 1997). Water molecules were added using the CCP4 WATPEAK program, but they were kept only if consistently positioned (by eye inspection) within the electron density map and if their B-factor was lower than 60 Å. Inspection of the protein structure with PROCHECK (Laskowski et al., 1993) showed that the geometry of the structure was satisfactory and consistent with the resolution of the starting data.

TABLE 1 Summary of data collection for crystals of Mb-YQR

Crystallographic Parameters	Deoxy	Oxy
Unique Reflections	19,614	26,633
Resolution (Å)	1.8	1.7
Completeness (%)	90.0	99.7
R-merge (%)	9.5	7.5
Space Group	P6	P6
Unit Cell		
a = b	91.50	90.33
c	45.98	45.24
R cryst. (%)	16.9	18.00

Kinetics

Overall rate constants with NO, O_2, and CO were obtained partly by stopped-flow (Applied Photophysics, DX.17 Mv, Leatherhead, UK), following standard procedures, and partly by laser photolysis. Time courses for geminate recombination were acquired following photolysis by a 9-ns flash at a wavelength of 532 nm from a YAG laser (Continuum Corp., Santa Clara, CA). Observation was usually at 436 nm, near the maximum of the oxy-deoxy difference spectrum; the signals were detected with a Hamamatsu R1913 (Hamamatsu Co., Bridgewater, NJ) photomultiplier and recorded with a Tektronix 7104 oscilloscope (Tektronix Co., Wilsonville, OR), charge-coupled camera, and video capture board in an IBM 486 computer. A more complete description of the apparatus was reported by Shibayama et al. (1995) and Scott and Gibson (1997). For experiments with xenon a stainless steel pressure cell with a gas volume of 4 ml, anti-reflection-coated sapphire windows, and a path length of 1 mm was employed. With O_2 as a ligand, data were collected in air and then with pure O_2 at 1 atm. Experiments with CO were performed by degassing, flushing the tonometer with CO, and finally adding a minimal amount of dithionite through a septum attached beyond the tonometer stopcock. Samples with NO were prepared from the same solution after collection of CO data by flushing the tonometer with N_2 and introducing 5 ml NO gas. This sample was equilibrated with the gas mixture, and when bimolecular reactions were followed, was allowed to stand for 5–10 min and reequilibrated to assure the removal of residual dithionite. For the experiments with xenon the same procedures were followed, with sample preparation in the pressure cell (see above); a vacuum pump and short metal tubes were used to connect the pressure cell to the xenon tank and pressure gauge after data had been collected in the absence of xenon.

Molecular dynamics

Simulations were run using the program MOIL with implementation of the locally enhanced sampling algorithm (Elber and Karplus, 1990; Elber et al., 1994). This provides multiple copies of the ligand, each influenced by the protein; the protein experiences the average forces of all ligands, which are invisible to each other. The cutoff radius for nonbonded interactions was 10 Å and the 1–4 scaling factors 2 for electrostatic and 8 for van der Waals interactions. All crystallographic water molecules were included and modeled as TIP3 (see Scott and Gibson, 1997). The crystal structure of wt oxy Mb (Phillips et al., 1990) or oxy Mb-YQR were used as a starting point. Runs with and without xenon were performed using the same distribution of initial velocities. The temperature of the protein was raised to room temperature over the first 15 ps.

RESULTS AND DISCUSSION

Structure of Mb-YQR by crystallography

Data collection statistics of the structure of the oxy and deoxy derivatives are given in Table 1; the limit of diffraction ranged from 1.7 to 1.8 Å. The crystallographic R factors ranged from 17% to 18%, with acceptable variations from ideal stereochemistry.

The 3D structure shows no significant differences with respect to wt Mb outside the regions where amino acid substitutions were introduced. When the superposition of the mutant with the wt structure was carried out, we observed changes smaller than those observed on comparing native Mb and recombinant wt Mb, the only exception being an ~1.4 Å displacement of Phe(CD4)46 observed in deoxy Mb-YQR. In this paper, all the comparisons with wt Mb have made use of the coordinates of the recombinant protein (Phillips et al., 1990). Structural information of Mb-YQR as the met cyanide derivative, obtained by ^{1}H-NMR (Zhang et al., 1997), allowed determination of the distal residues orientations. In this derivative, distal Tyr(B10)29 provides a strong H-bond to the bound cyanide, but also distal Gln(E7)64 is close enough to the ligand to serve as an H-bond donor.

The electron density maps of the ligand binding pocket of the oxy and deoxy derivatives of Mb-YQR, given in Fig. 1,

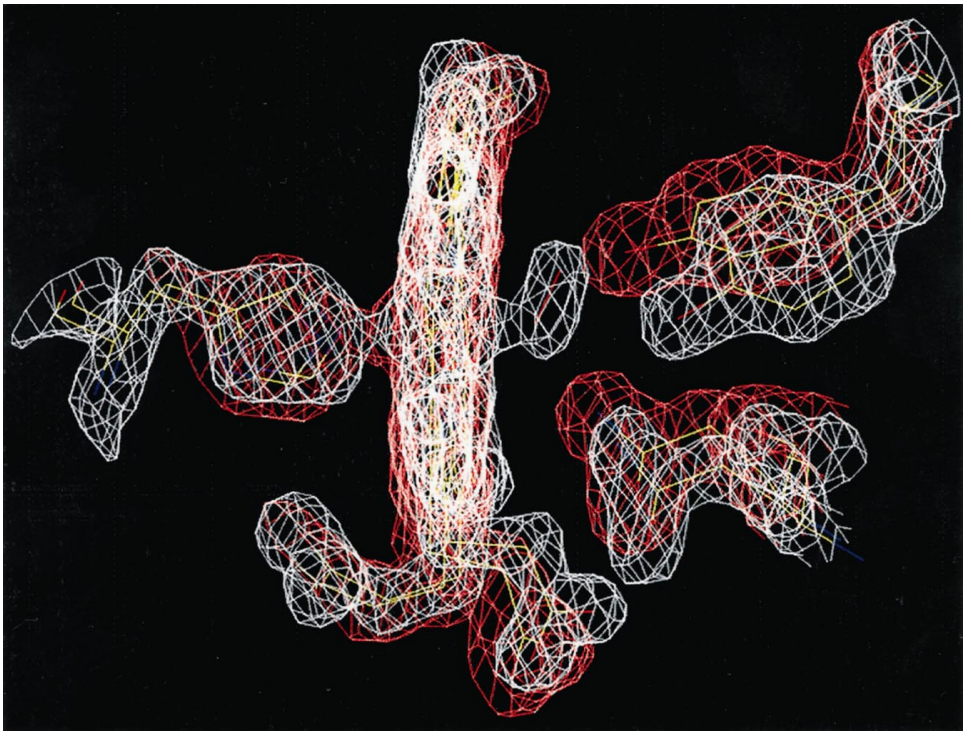

FIGURE 1 Superposition of the electron density maps of oxy (*white*) and deoxy (*red*) Mb-YQR. Proximal His(F8) is shown on the left, and the mutated distal residues Tyr(B10) and Gln(E7) on the right. Bound O_2, shown as a red bar, corresponds to an Fe–O1–O2 bond angle of 115.0°. The displacement of the hydroxyl group of Tyr(B10)29, observed after superposition of the oxy and deoxy structures, is 1.75 Å. The distance of the hydroxyl group from the heme iron is 4.5 Å in deoxy and 4.9 Å in oxy Mb-YQR.

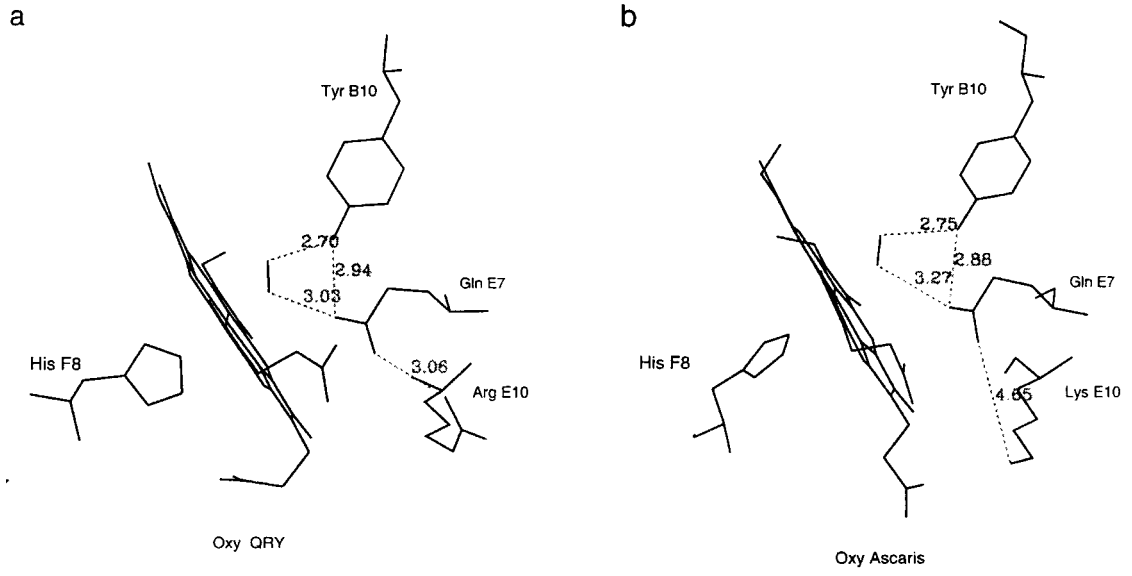

FIGURE 2 Structure of oxygenated Mb-YQR (*a*) and *Ascaris* Hb (*b*). The figure shows the mutated residues, the heme, bound dioxygen, and the proximal His(F8) of Mb-YQR (*a*), and equivalent residues in *Ascaris* Hb domain I (*b*). Interatomic distances, shown as dotted lines, are given in angstroms.

show that the H-bonding partners to O_2 are different from those observed in wt Mb, where the distal His at position E7 is H-bonded to dioxygen (Perutz, 1989; Phillips et al., 1990). In oxy Mb-YQR we observed a structure that closely mimics the binding pocket of *Ascaris* Hb domain I (Yang et al., 1995) as far as the H-bonding pattern is concerned (Fig. 2). In fact, the main H-donor to the ligand is the hydroxyl group of Tyr(B10)29, with a distance of 2.7 Å (2.7 Å in *Ascaris* Hb); a second, bifurcated H-bond is contributed by the amino group of Gln(E7)64 with a distance from the O1 of bound dioxygen of 3.0 Å (3.3 Å in *Ascaris* Hb) and a distance 2.94 Å from the hydroxyl group of Tyr(B10)29 (2.88 Å in *Ascaris* Hb) (Fig. 2). A rotation around the bond C—C (γ) brings the Tyr(B10)29 hydroxyl to a distance of 2.7 Å from the O2 of dioxygen, which has an angle (Fe–O1–O2) close to wt oxy Mb (115.0° vs. 118.2°); however, the position of O2 is displaced by 1.3 Å and is orthogonal with respect to wt Mb, pointing toward CHD (see Fig. 3). The Tyr can be accommodated in the distal pocket with small changes in the C_α position with respect to wt Mb (0.48 Å), and with only 0.1 Å displacement with respect to the C_α of position B10, as reported in the structure of the oxygenated mutant Mb Leu(B10) $\rightarrow$ Phe (Carver et al., 1992).

The carbonyl group of Gln(E7)64 may have some electrostatic interaction with Arg(E10)67 being at a distance of 3.06 Å in oxy and 3.1 Å in deoxy Mb-YQR (Fig. 2). This interaction is absent in *Ascaris* Hb, since the amino group of Lys(E10) is too distant, being 4.65 Å away (Yang et al., 1995). The former interaction is probably labile, since the terminal part of the Arg side chain is not well defined in the electron density maps of both oxy and deoxy Mb-YQR. This side chain was also shown to be mobile in the structure of the cyanide derivative of met Mb-YQR determined by high-resolution NMR (Zhang et al., 1997). Therefore it is unlikely that Arg at position E10 plays a major or even a significant role in the stabilization of the iron-bound ligand.

As shown in Fig. 1, comparison of oxy and deoxy Mb-YQR shows a fairly large mouvement of both Tyr(B10)29 and Gln(E7)64 upon O_2 binding. This corresponds to a shift in the position of the hydroxyl group of Tyr(B10)29 of 1.75 Å, and it involves a swinging motion of this residue. In deoxy Mb-YQR, the distance of the hydroxyl group of Tyr(B10)29 from the position occupied by the O2 atom in

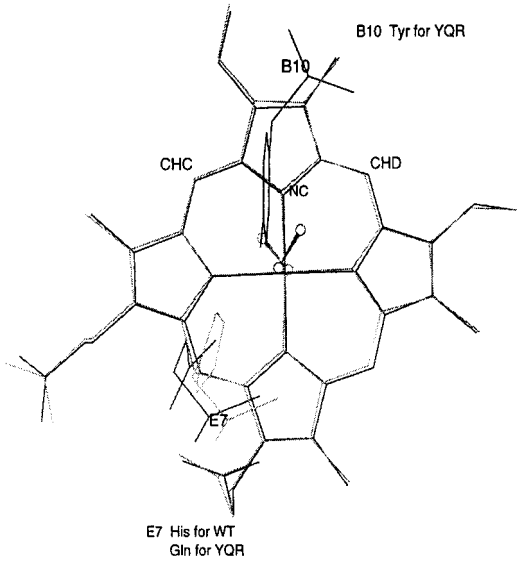

FIGURE 3 Superposition of the heme, of residue (E7), and dioxygen for the oxygenated derivatives of wild-type Mb (*thin lines*) and Mb-YQR (*heavy lines*). Tyr(B10) in Mb-YQR is also shown. Dioxygen is represented as ball-and-stick model.

oxy Mb-YQR would be only 1.56 Å, implying steric clash. While in the deoxygenated state of wt Mb a water molecule is found in the distal pocket (Phillips et al., 1990), this was not detected in deoxy or oxy Mb-YQR.

Overall binding constants

Table 2 reports the overall rate constants for the binding and dissociation of NO, O_2, and CO by the proteins examined in this paper. It was already reported (Travaglini-Allocatelli et al., 1994) that the O_2 dissociation rate constant of Mb-YQR is decreased compared to wt Mb, but still much faster than that unique to *Ascaris* Hb. The observed decrease in O_2 dissociation rate is obviously consistent with the increased H-bonding potential of the distal site of Mb-YQR compared to wt. No effect was detected on the dissociation rate of CO given that the rate-limiting barrier to dissociation of this ligand is the Fe-ligand bond breaking (Zhang et al., 1997; Springer et al., 1994). While the rate for CO binding was determined by stopped-flow (Travaglini-Allocatelli et al., 1994), the rates for O_2 and NO were determined in this work by laser photolysis; in all cases second-order kinetics was obeyed. The data (Table 2) show that while the rate constant for NO binding is unchanged compared to wt Mb, the rates for O_2 and CO are 10-fold smaller. The combination rate constants to Mb-YQR were found to be the same at pH 7 (in phosphate) and pH 9.1 (in 2% borate) for both O_2 and NO.

Photolysis experiments

No geminate reaction was detected with both CO and O_2, which implies this to be well below 5%. While the result with CO was expected, the result with O_2 is highly unusual and very interesting, Scott and Gibson (1997) reporting for 25 sperm whale Mb mutants nanosecond geminate recombination ranging between 30 and 50% of the total amplitude. Fifty percent of the bound O_2 was removed from oxy Mb-YQR by the 9-ns laser flash, against 80–90% from wt Mb, but after a few microseconds the amount of dissociated ligand is similar for both proteins. This is because in Mb-YQR the dissociated ligand diffuses away from the iron, against 60% for wt. This behavior is strikingly different from that of *Ascaris* Hb, where relatively little O_2 escaped to solution and a prominent picosecond geminate reaction with O_2 was observed (Gibson et al., 1993).

The sensitivity to photolysis of ligands bound to Mb-YQR is expressed in Fig. 4 as the fraction of photodissociated Mb against relative light intensity. These data show that while for Mb-YQR the apparent quantum yield for O_2 (6.7%) is not very different from that of wt Mb, that for NO is 50-fold higher. Earlier data for *Ascaris* Hb (Gibson et al., 1993) showed the yield for O_2 to be 1000-fold smaller, and that for NO 10-fold smaller than wt Mb. Therefore, the yield for NO in Mb-YQR (~4%) is much larger than for *Ascaris* Hb (~0.01%), a gigantic increase of ~400-fold, which points to important structural differences.

Approximately 40% of NO bound to Mb-YQR was dissociated by the 9-ns laser flash, a quota much higher than the 1–3% dissociation seen with wt Mb under the conditions of the experiment (Gibson et al., 1993). This photolability permitted the first accurate determination ever made of the time course of geminate rebinding of NO; indeed, ~30% of the dissociated ligand was found to recombine in a geminate reaction that showed two prominent nanosecond components (Fig. 5 *A*). The time course of this reaction was analyzed in terms of the branched model used by Chatfield et al. (1990) and by Scott and Gibson (1997). This reaction scheme, also shown in Fig. 5, proposed that the immediate photoproduct may either escape to the solution or migrate to a "secondary site" adjacent to the heme pocket, eventually returning later to the "primary site" and recombining with the iron. The time course in Fig. 5 and the parameters of the fit, given in the legend to Fig. 5, show that for Mb-YQR the proportion of the very slow geminate reaction is high indeed. A direct comparison with analogous NO data for wt Mb is not possible because (as reported above) too little NO is photodissociated in the latter case to allow a detailed analysis. Comparisons can, however, be made with the O_2 data of Scott and Gibson (1997), and show that the slow

TABLE 2 Overall rate constants for the reaction of NO, O_2, and CO with wt Mb, Mb-YQR, and *Ascaris* Hb

	k_{on} (μM^{-1} s^{-1})			k_{off} (s^{-1})		
Protein	NO	O_2	CO	NO	O_2	CO
Mb-LHT[a] (wt)	20	15	0.55	0.001	14	0.019
Mb-YQR[a]	20	2	0.04	—	1	0.014
Ascaris Hb	5	1.5	0.21	—	0.004	0.01

Data from Antonini and Brunori (1971), Gibson and Smith (1965), Gibson et al. (1993), Travaglini-Allocatelli et al. (1994), and this work.

[a]The a.a. single-letter codes indicate amino acids that occupy positions B10, E7, and E11 from left to right.

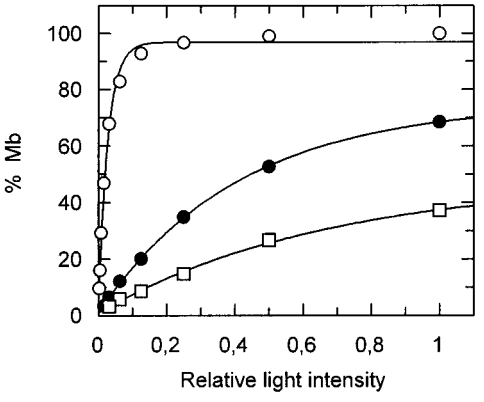

FIGURE 4 Determination of the photodissociation efficiency for Mb-YQR-O_2 and Mb-YQR-NO, relative to wt Mb-CO. Dependence of the percent of deoxy Mb obtained by photodissociation with a 9-ns laser pulse, as function of relative light intensity. Continuous lines are best fit to a single exponential. Data for wt Mb CO (○), with μs quantum yield of 1; data for oxy Mb-YQR (●), with μs quantum yield of 0.067; data for nitrosyl Mb-YQR (□), with μs quantum yield of 0.042.

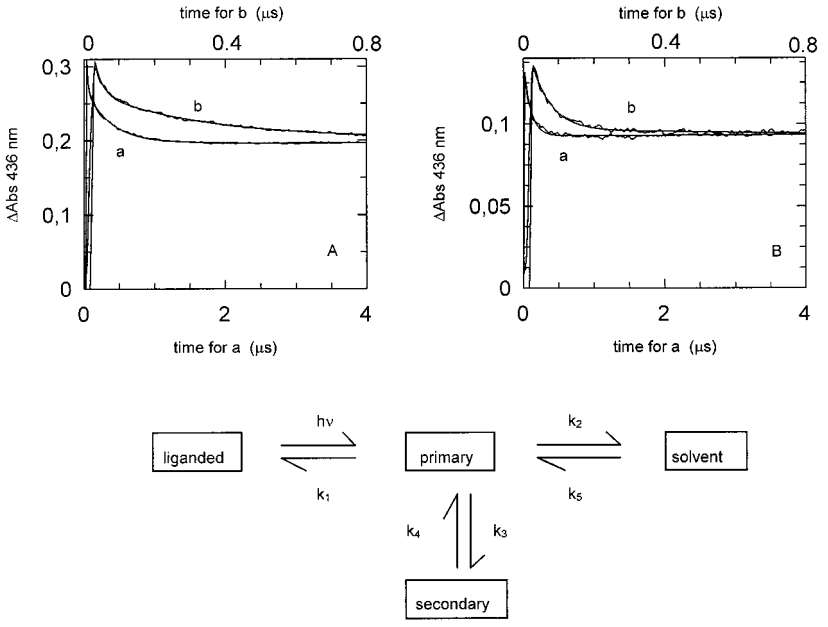

FIGURE 5 Geminate rebinding of NO to Mb-YQR. Panel (*A*) shows the time course of NO geminate rebinding after laser photolysis of Mb-YQR. Traces *a* and *b* refer to the lower and upper time scales. Continuous lines are the best fit according to the scheme shown below, with the following values for the rate constants (in μs^{-1}): $k_1 = 17$; $k_2 = 19$; $k_3 = 19$; $k_4 = 4.5$ (see Scott and Gibson, 1997). Notice the prominent slow-phase of geminate rebinding seen clearly in trace b of panel *A*. Panel (*B*) shows the same experiment as in (*A*) but in the presence of 12 atm of xenon. Fit yielded the following values for the rate constants (in μs^{-1}): $k_1 = 12$; $k_2 = 16$; $k_3 = 6$; $k_4 = 10$. Notice that the amplitude of the slow phase is very much decreased, as may be seen comparing traces *b* in the two panels; moreover, the total excursion (shown as the absorbance change at 436 nm) is less than one-half in the presence of xenon (see text).

component for NO seen with Mb-YQR is two to three times larger than in the mutants they studied; thus this particular triple mutant shows, once again, quite unusual intramolecular ligand binding kinetics.

Scott and Gibson (1997) also showed that high partial pressures of xenon increased the rate and amplitude of the faster geminate phase, while diminishing or abolishing the slower one. This result was interpreted to mean that photodissociated O_2 migrates to some of the xenon binding sites (Tilton et al., 1984), which may therefore be associated with the origin of the slow geminate phase. In the case of Mb-YQR, a pressure of 12 atm of xenon considerably reduced the contribution of the slower NO geminate phase while increasing the fraction of the rapid phase, as shown in Fig. 5 *B*. It is concluded that a large proportion of photodissociated NO in Mb-YQR may migrate into one of the xenon sites, giving rise to the slower geminate phase, and correlating with the unusually high quantum yield for NO.

In nanosecond photolysis experiments with O_2 and NO in the presence of 12 atm of xenon a large decrease in the total absorbance excursion was also observed; this may be taken as a measure of the relative ease with which O_2 can recombine with the iron atom or diffuse into a xenon site (Tilton et al., 1984). The change in absorbance of 34% seen for O_2 in Mb-YQR is several times larger than the effects seen by Scott and Gibson (1997) with other mutants, and taken together with the still larger decrease of 55% in the amplitude seen for NO, suggests that O_2 and NO find greater difficulty in approaching the iron in Mb-YQR than in many other Mb mutants. Assuming similar diffusion coefficients for all the diatomic gases, it seems relatively easy for them to fill the xenon site(s); this interpretation is consistent with the MD simulations on Mb-YQR showing ligand molecules diffusing to the Xe(4) site, as discussed below.

Molecular dynamics simulations

The coordinates of oxy Mb-YQR were used as a starting point in simulation runs that extended to 50 ps. Ligand diffusion showed three distinct patterns determined by the initial distribution of atomic velocities. In five of eight runs the ligand cloud remained close to its starting point and was tightly constrained by Tyr(B10)29, Phe(CD1)43, Gln(E7)64, Val(E11)68, and the heme group, with a ligand atom spending, on average, 80% of the time within 4 Å of the iron atom; the mean separation of the centers of ligands was 0.51 Å, and did not change significantly throughout the run. It may be appreciated that residues at (B10), (CD1), (E7), and (E11) were identified by crystallography of the photolytic intermediate of wt Mb to confine the position of dissociated CO in the distal heme pocket, as outlined in the Introduction (Schlichting et al., 1994; Teng et al., 1994; Srajer et al., 1996). Two runs began with much the same appearance, but after 10 ps or so the δ-carbon atom of Ile(G8)107, which normally points toward Tyr(B10)29, swung around opening a path communicating with the Xe(4) site of Tilton et al. (1984), a site defined by Gly(B6)25, Ile(B9)28, Tyr(B10)29, Val(E11)68, and Ile(G8)107, 8.5 Å above the iron (see Fig. 6). The path was taken by all the ligand copies in one run, and by 7 copies (of 10) in the other. After this translation, the ligand group was confined by Gly(B6)25, Ile(B9)28, Val(E11)68, Leu(E12)69, and Ile(G8)107 with much the same mean distance between ligand centers as before. Clearly this docking site is different from that identified by crystallography of the photolytic intermediate of Mb (see above). In a single run, Tyr(B10)29 swung upward, the long axis of the aromatic ring becoming more nearly parallel to the plane of the heme; this allowed the ligand group to move upward beneath the ring of Tyr(B10)29 to a mean distance of 5–6 Å

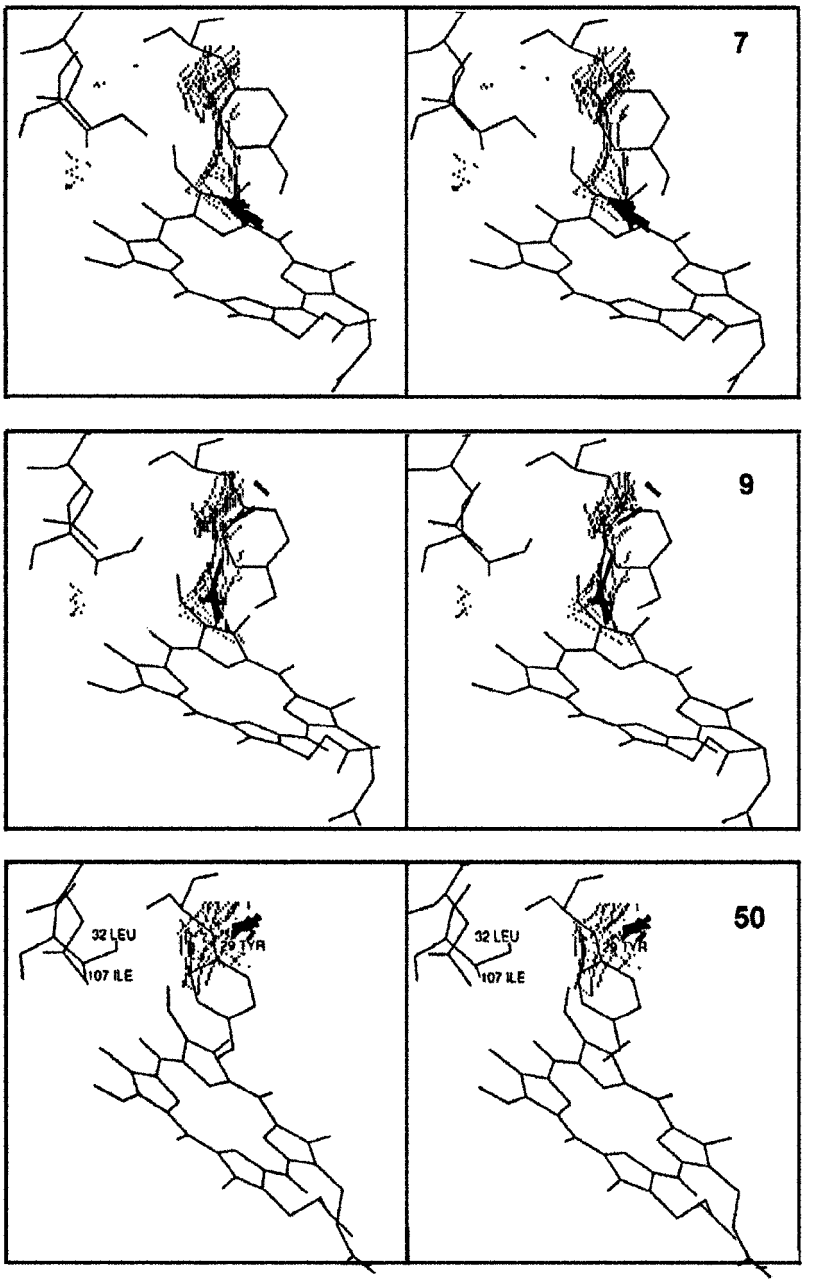

FIGURE 6 Molecular dynamics simulations of Mb-YQR. Stereo stick diagrams showing trajectories of photodissociated ligand (10 copies shown by heavy bars) at 7, 9, and 50 ps from top to bottom, and the openings tracing the path and space able to accommodate a ligand, as indicated by dots. Tyr(B10)29 introduced in Mb-YQR is shown together with Ile(G8)107, which changes configuration between 7 and 9 ps, opening access to the "secondary site" beneath Tyr(B10)29.

from the iron; in this case, there was no coordinated movement of Ile(G8)107. Runs that included xenon atoms in the four main sites of Tilton et al. (1984) suggest that the pathway beneath Tyr(B10)29 and Ile(G8)107 should be effectively blocked by xenon in the site (4), which occupies the space illustrated in Fig. 7 (*top*).

These simulations, together with the results of the geminate experiments, may be taken to suggest that in Mb-YQR ligands readily leave the vicinity of the iron, moving upward to a "secondary site" overlapping the Xe(4) site, and returning partially toward the iron to generate the large slow geminate recombination reaction shown in Fig. 5 *A*. The unusually high apparent microsecond quantum yield for NO (~4%) may also be related to the ease of transit of ligands away from the iron, gated by Ile(G8)107. The effect of high partial pressures of xenon in abolishing the slow reaction of NO is immediately explained by the result shown in Fig. 7 (*top*). The other effect of xenon (i.e., an increase in the rate and amplitude of the faster geminate reaction) may also be attributed to occupancy of this docking site, as the faster recombination reaction no longer must compete with escape from the vicinity of the iron. The same explanation may account for the decrease in the apparent microsecond quantum yield brought about by xenon (see Kinetics).

If the same mechanism applies to O_2 and CO, xenon would be expected to induce a geminate reaction with these ligands, but only a small reaction was seen with O_2 and, of course, none with CO. These results, together with the

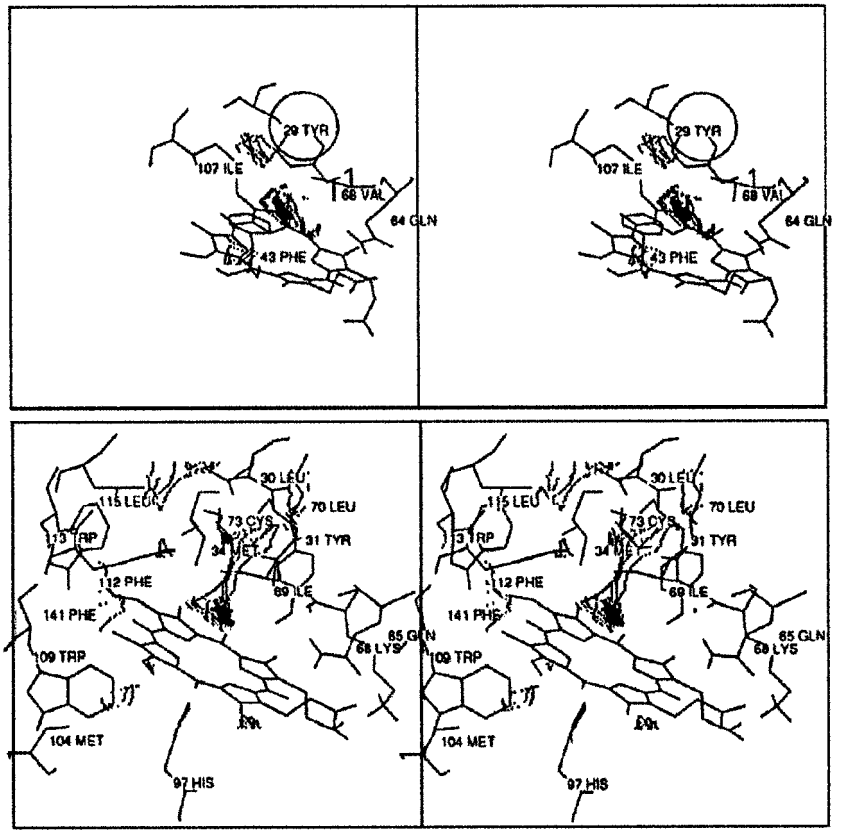

FIGURE 7 Molecular dynamics simulations of Mb-YQR and *Ascaris* Hb. Top panels show the simulation of Mb-YQR in the presence of xenon at site 4 of Tilton et al. (1984): it may be seen that the photodissociated ligand is confined near the heme since the "secondary site" is blocked by xenon (shown as a large circle). Bottom panels show the simulation of *Ascaris* Hb (domain I, coordinates from Yang et al., 1995) with photodissociated ligand confined near the metal, in agreement with the geminate recombination kinetics (Gibson et al., 1993). The topological position G8 is occupied by the ring of Phe(112), which may be seen edge-on (to the left) blocking access to a position analogous to the "secondary site."

reduced values of the overall bimolecular rate constants (Table 2), suggest that the rate of reaction of these two gases at the iron is significantly decreased compared to wt Mb. This suggestion is fortified by the result of the second-order rate constant for NO, which is the same as for wt (Table 2); the implication is that diffusion into the heme pocket is unchanged in Mb-YQR, a plausible result in view of the structural information reported above. As the diffusion constants for all three gaseous ligands are closely similar, the lower rates for O_2 and CO cannot be attributed to difficulty in entering the protein.

An attempt has been made to compare Mb-YQR with *Ascaris* Hb in the hope of explaining the large difference (250-fold) in the rate of O_2 dissociation from these two proteins. The same problem has been addressed by Peterson et al. (1997) to account for the kinetic properties of *Lucina pectinata* Hb-II vis-a-vis those of *Ascaris s.* Hb, given the identity of residues (B10) and (E7) in the two proteins. The simulations for *Ascaris* Hb shown in Fig. 7 (*bottom*) suggest that the kinetic difference with Mb-YQR may be due to the presence of Phe at position 112 in the *Ascaris* sequence (the corresponding residue being Ile(G8)107 in wt Mb and Mb-YQR). As may be seen in Fig. 7, the aromatic ring of Phe(G8)112 is placed to obstruct the pathway between the immediate heme pocket and the cavity corresponding to the Xe(4) site, preventing the escape of ligands from the "primary site" and resulting in an apparent low rate of thermal dissociation because of enhanced recapture by the iron. Thus the Phe ring has an effect analogous to that of Xe(4) in Mb-YQR, depicted in Fig. 7 (*top*). In addition to its effect in lowering the apparent O_2 dissociation rate, Phe(G8)112 may account for the unusually large picosecond geminate reaction of *Ascaris* Hb with O_2, as well as its nanosecond geminate reaction and the low apparent quantum yield with both O_2 and NO, as discussed above (see Gibson et al., 1993). In their analysis of the kinetic properties of *Ascaris s.* Hb and *Lucina p.* Hb-II, Peterson et al. (1997) suggested that O_2 dissociation in the former protein may demand large amplitude fluctuations of the tight distal site coupled to rupture of the H-bond between bound O_2 and the distal residues shown by the crystallographic structure (Yang et al., 1995). It is interesting to point out that in *Lucina p.* Hb-II the residue at position (G8) is Ala (Hockenhull-Johnson et al., 1991).

CONCLUDING REMARKS

The more general conclusion emerging from the data reported above relates to the fundamental significance of detailed structural dynamics for the interpretation of biochemically relevant functional data. Even when starting from the high resolution structure of the reactant and product, in our case the deoxy and oxy derivatives of a triple mutant of sperm whale Mb (Leu(B10) → Tyr; His(E7) → Gln; Thr(E10) → Arg), understanding the molecular basis

of ligand reactivity demanded an investigation over a very wide dynamic range, both experimental and theoretical. This mutant (called Mb-YQR) was designed and expressed to simulate and reproduce the kinetics of the O_2 reaction observed for *Ascaris* Hb (Davenport, 1949), with the idea to improve engineering of a hemoglobin to be used as a "blood substitute" (Travaglini-Allocatelli et al., 1994). Interpretation of the nanosecond laser photolysis recombination data in the light of MD simulations permits several conclusions of general interest, going well beyond the original purpose of the project.

As shown in Table 2, the rate of O_2 dissociation from Mb-YQR is slower than that of wt Mb, but still ~250 fold faster than *Ascaris* Hb. The role of the H-bond between His(E7)64 and bound O_2 in controlling the rate of dissociation in wt Mb was unequivocally shown by site-directed mutagenesis (Olson et al., 1988). Since the two H-bonds established by Tyr(B10)29 and Gln(E7)64 with bound O_2 are essentially identical in Mb-YQR and *Ascaris* Hb (Fig. 2), the unique slow rate of the latter is difficult to understand. The geminate recombination data with NO and the effect of xenon (Fig. 5), together with MD simulations (Fig. 6), converge in suggesting a dynamic pathway for thermal ligand dissociation and escape, which may account for the difference between Mb-YQR and *Ascaris* Hb. In the former case, a conspicuous "secondary site" beneath Tyr(B10)29, where ligands can diffuse, is made accessible by the swinging of Ile(G8)107, as indicated in Fig. 6; the presence in *Ascaris* Hb of Phe at the same topological position (position 112 in its sequence) effectively blocks access to this "secondary site," which corresponds to the pocket occupied by xenon in the so-called site (4) of Tilton et al. (1984), and which is clearly different from the docking site identified by crystallography of the photolytic intermediate of wt Mb (Schlichting et al., 1994; Teng et al., 1994; Srajer et al., 1996). Therefore, the kinetic barrier for O_2 dissociation in Mb-YQR (which is already higher than wt Mb by ~2 kcal mol^{-1}) should increase if Ile(G8)107 is mutated to Phe, effectively blocking access to the "secondary site" and thereby considerably increasing the probability of O_2 recapture by the iron. This structural interpretation of the data is consistent with the striking difference in the microsecond quantum yield for NO as between Mb-YQR and *Ascaris* Hb, with an increase of ~400-fold to a value never observed before, and agrees with the absence of O_2 geminate recombination vis-a-vis the conspicuous geminate picosecond phase seen in *Ascaris* Hb (Gibson et al., 1993). Moreover, it implies that in Mb-YQR the ligand may diffuse from the "secondary site" out in the solvent, indicating a possible dynamic pathway different from the one presumed to be dominant in wt Mb (i.e., the so-called His(E7)64 gate; Olson and Phillips, 1996; Springer et al., 1994). The case represented by Mb-YQR is but one of the possible escape pathways identified by Huang and Boxer (1994) using random mutagenesis of human Mb. The consistency of this interpretation with the data on Mb-YQR provides strong support for the hypothesis that the protein channel identified by laser photolysis experiments is also used in the thermally activated reactions, thereby increasing the general significance of the photochemical kinetic experiments. Moreover, our interpretation extends the hypothesis put forward by Peterson et al. (1997) to account for the kinetic behavior of *Lucina p.* Hb-II which, despite Tyr at (B10) and Gln at (E7), has an O_2 dissociation rate constant ($k = 0.11\ s^{-1}$) higher than *Ascaris* Hb (Kraus and Wittenberg, 1990).

Examination of the combination rate constants, also summarized in Table 2, provides an opportunity for considerations about reactivity of a hemeprotein, with some aspects of originality. If we take as a frame of reference a two-barrier/three-state model for ligand binding and dissociation (Fig. 8), the rate constant for NO combination implies that the outer barrier in Mb-YQR is unchanged compared to wt Mb. Thus the reduced O_2 and CO combination rate constants observed for Mb-YQR (10-fold) cannot be accounted for on the basis of an increased diffusion barrier nor is it expected that proximal effects may come into play, given that there are no detectable perturbations in the stereochemistry of the iron porphyrin-protein contacts on the proximal side compared to wt Mb. The most plausible hypothesis to account for the reduction in the overall combination rate constants for O_2 and CO in Mb-YQR is based on the observation illustrated in Figs. 1 and 3, where the structure

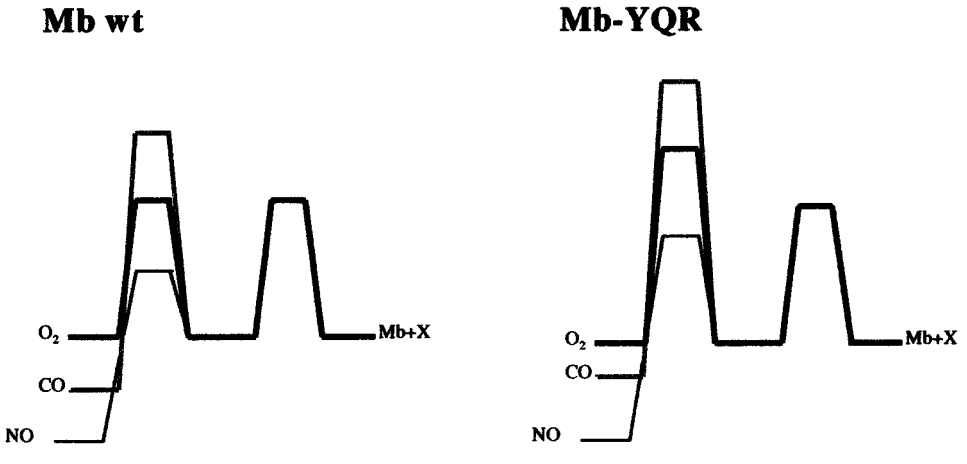

FIGURE 8 Energy profile for ligand (O_2, CO, NO) binding to wt Mb and Mb-YQR, according to a three states/two barriers model (Olson and Phillips, 1996). The "external" barrier (shown at the right) is the same in all cases, and changes in the "internal" barrier are highlighted for the three gases (see text).

of the active site in the oxy and deoxy derivatives can be seen. The prominent results from the crystallographic model are (1) the substantial movement of Tyr(B10)29 and Gln(E7)64 in the deoxygenated Mb-YQR whereby they tend to occupy the space left free by O_2 removal; (2) the absence of a water molecule in either ligation state, contrary to wt deoxy Mb (Phillips et al., 1990); and (3) the unusual orientation of bound O_2, which is orthogonal to the position occupied in wt Mb (Fig. 3). It seems that the additional constraints imposed in the mutant by the new distal site may well account for the 10-fold reduction in combination rate, as both O_2 and CO will spend some of the favorable free energy originating by bonding to the iron in acquiring space and correct geometry in the Mb-YQR distal site. If this interpretation is correct, it may be of interest to compare the kinetics of ligand binding to R- and T-state Hb-YQR, and it is expected that the transition state for NO binding will be shifted along the reaction coordinate from "reactant-like" to "product-like" (Szabo, 1978; Henry et al., 1997). Thus the overall combination time course of O_2 and NO to deoxy Hb will be slower and possibly autocatalytic, at variance with human HbA, where the rate of binding of these two gases (contrary to CO) is largely independent of allosteric state (Antonini and Brunori, 1971).

In summary, the new data on Mb-YQR show very clearly that availability of a high-resolution 3D structure of the reactant and product (in this case oxy and deoxy Mb-YQR) is a necessary but insufficient condition for understanding the functional control of ligand binding, and that dynamics has to be brought into the picture to propose a plausible detailed mechanism, which may explain the biochemically relevant rate and equilibrium constants. If very fast fluctuations of internal amino acid side chains control the overall rate of O_2 dissociation, they acquire general significance for the physiology of O_2 delivery to tissues, and therefore may have *survival value*.

The authors are very grateful to Prof. D. Tsernoglou (Rome, Italy), for his crucial role in establishing the Protein Crystallography Unit at the University of Rome "La Sapienza." The invaluable help of Dr. J. Tame (York, UK) in structural computation is gratefully acknowledged. We thank Dr. L. Nicolini and Mr. R. Dagai (Istituto Superiore di Sanità, Rome, Italy) for their help with large-scale *E. coli* fermentations.

This work was partially supported by grants from the MURST of Italy (P. N. "Biologia strutturale," 1997), from the Agenzia Spaziale Italiana of Italy, and United States Public Health Service Grant GM 14276 (to Q.H.G.).

REFERENCES

Antonini, E., and M. Brunori. 1971. Hemoglobin and myoglobin in their reactions with ligands. North Holland Publishing, Amsterdam.

Austin, R. H., K. W. Beeson, J. Eisenstein, H. Frauenfelder, and I. C. Gunsalus. 1975. Dynamics of ligand binding to myoglobin. *Biochemistry.* 14:5355–5373.

Carver, T. E., R. E. Brantley, Jr., E. W. Singleton, R. M. Arduini, M. L. Quillin, G. N. Phillips, Jr., and J. S. Olson. 1992. A novel site-directed mutant of myoglobin with an unusually high O_2 affinity and low autooxidation rate. *J. Biol. Chem.* 267:11443–14450.

Chatfield, M. D., K. N. Walda, and D. Magde. 1990. Activation parameters for ligand escape from myoglobin proteins at room temperature. *J. Am. Chem. Soc.* 112:4680–4687.

Collaborative Computional Project, Number 4. The CCP4 suite: programs for protein crystallography. 1994. *Acta Crystallogr. D.* 50:760–763.

Davenport, H. E. 1949. Hemoglobins of *Ascaris lumbricoides. Proc. R. Soc. Lond. Biol. Sci.* 136:255–270.

De Baere, I., M. F. Perutz, L. Kiger, M. C. Marden, and C. Poyart. 1994. Formation of two hydrogen bonds from the globin to the heme-linked oxygen molecule in *Ascaris* hemoglobin. *Proc. Natl. Acad. Sci. USA.* 91:1594–1597.

Elber, R., and M. Karplus. 1990. Enhanced sampling in molecular dynamics: use of the time-dependent Hartree approximation for a simulation of carbon monoxide diffusion through myoglobin. *J. Am. Chem. Soc.* 112:9161–9175.

Elber, R., A. Roitberg, C. Simmerling, R. F. Goldstein, G. Verkhiver, H. Li, and A. Ulitsky. 1994. Statistical Mechanics, Protein Structure and Protein Substrate Interactions. S. Doniach, editor. Plenum Press, New York.

Frauenfelder, H., N. A. Alberding, A. Ansari, D. Braunstein, B. R. Cowen, M. K. Hong, I. E. T. Iben, J. B. Johnson, S. Luck, and M. C. Marden. 1990. Proteins and pressure. *J. Phys. Chem.* 94:1024–1037.

Gibson, Q. H. 1989. Hemoproteins, ligands, and quanta. *J. Biol. Chem.* 264:20155–20158.

Gibson, Q. H., R. Regan, J. S. Olson, T. E. Carver, B. Dixon, B. Pohajdak, P. K. Sharma, and S. N. Vinogradov. 1993. Kinetics of ligand binding to *Pseudoterranova decipiens* and *Ascaris suum* hemoglobins and to Leu29 → Tyr sperm whale myoglobin mutant. *J. Biol. Chem.* 268: 16993–16998.

Gibson, Q. H., and M. H. Smith. 1965. Ligand binding kinetics to A. lumbricoides. *Proc. R. Soc. Lond. B.* 163:206–214.

Henry, E. R., C. M. Jones, J. Hofrichter, and W. A. Eaton. 1997. Can a two-state MWC allosteric model explain hemoglobin kinetics? *Biochemistry.* 36:6511–6528.

Hockenhull-Johnson, J. D., M. S. Stern, P. Martin, C. Dass, D. M. Desiderio, J. B. Wittenberg, S. N. Vinogradov, and D. A. Walz. 1991. The amino acid sequence of hemoglobin II from the symbiont-harboring clam *Lucina pectinata. J. Protein Chem.* 10:609–622.

Hofrichter, J., J. H. Sommer, E. R. Henry, and W. A. Eaton. 1983. Nanosecond absorption spectroscopy of hemoglobin. Elementary processes in kinetic cooperativity. *Proc. Natl. Acad. Sci. USA.* 80: 2235–2239.

Huang, X., and S. G. Boxer. 1994. Discovery of new ligand binding pathways in myoglobin by random mutagenesis. *Nature Struct. Biol.* 1:226–229.

Kraus, D. W., and J. B. Wittenberg. 1990. Hemoglobins of the *Lucina pectinata*/bacteria symbiosis. I. Molecular properties, kinetics and equilibria of reactions with ligands. *J. Biol. Chem.* 265:16043–16053.

Laskowsky, R. A., M. W. MacArthur, D. S. Moss, and J. M. Thornton. 1993. PROCHECK: a program to check the stereochemical quality of protein structures. *J. Appl. Crystallogr.* 26:283–291.

Murshdov, G., A. Vagin, and E. Dodson. 1997. Application of maximum likelihood methods for macromolecular refinement. *Acta Crystallogr. D* 53:240–255.

Olson, J. S., A. J. Mathews, R. J. Rohlfs, B. A. Springer, K. D. Egeberg, S. G. Sligar, J. Tame, J. P. Renaud, and K. Nagai. 1988. The role of distal histidine in myoglobin and haemoglobin. *Nature.* 336:265–266.

Olson, J. S., and G. N. Phillips, Jr. 1996. Kinetic pathway and barriers for ligand binding to myoglobin. *J. Biol. Chem.* 271:17593–17596.

Otwinowsky, Z., and W. Minor. 1996. Processing of x-ray diffraction data collected in oscillation mode. *Methods Enzymol.* 276:307–325.

Perutz, M. F. 1989. Myoglobin and haemoglobin: role of distal residues in reactions with haem ligands. *Trends Biochem. Sci.* 14:42–44.

Peterson, E. S., S. Huang, J. Wang, L. M. Miller, G. Vidugiris, A. P. Kloeck, D. E. Goldberg, M. R. Chance, J. B. Wittenberg, and J. M. Friedman. 1997. A comparison of functional and structural consequences of the tyrosine B10 and glutamine E7 motifs in two invertebrate hemoglobins (*Ascaris suum* and *Lucina pectinata*). *Biochemistry.* 36: 13110–13121.

Phillips, G. N., Jr., R. M. Arduini, B. A. Springer, and S. G. Sligar. 1990. Crystal structure of myoglobin from a synthetic gene. *Proteins.* 7:358–365.

Schlichting, I., J. Berendzen, G. N. Phillips, Jr., and R. M. Sweet. 1994. Crystal structure of photolysed carbonmonoxy-myoglobin. *Nature.* 371: 808–812.

Scott, E. E., and Q. H. Gibson. 1997. Ligand migration in sperm whale myoglobin. *Biochemistry.* 36:11909–11917.

Shibayama, N., T. Yonetani, R. Regan, and Q. H. Gibson. 1995. Mechanism of ligand binding to Ni(II)-Fe(II) hybrid hemoglobins. *Biochemistry.* 34:14658–14667.

Springer, B. A., S. G. Sligar, J. S. Olson, and G. N. Phillips, Jr. 1994. Mechanisms of ligand recognition in myoglobin. *Chem. Rev.* 94: 699–714.

Srajer, V., T. Teng, T. Ursby, C. Pradervand, Z. Ren, S. Adachi, W. Schildkamp, D. Bourgeois, M. Wulff, and K. Moffat. 1996. Photolysis of the carbon monoxide complex of myoglobin: nanosecond time-resolved crystallography. *Science.* 274:1726–1729.

Szabo, A. 1978. Kinetics of hemoglobin and transition state theory. *Proc. Natl. Acad. Sci. USA.* 75:2108–2111.

Teng, T. Y., V. Srajer, and K. Moffat. 1994. Photolysis-induced structural changes in single crystals of carbonmonoxy myoglobin at 40 K. *Nature Struct. Biol.* 1:701–705.

Tilton, R. F., I. D. Kuntz, and J. A. Petsko. 1984. Cavities in proteins: structure of a metmyoglobin-xenon complex solved to 1.9 Å resolution. *Biochemistry.* 23:2849–2857.

Travaglini-Allocatelli, C., F. Cutruzzolà, A. Brancaccio, B. Vallone, and M. Brunori. 1994. Engineering *Ascaris* hemoglobin oxygen affinity in sperm whale myoglobin: role of tyrosine B10. *FEBS Lett.* 352:63–66.

Yang, J., A. P. Kloek, D. E. Goldberg, and F. S. Mathews. 1995. The structure of *Ascaris* hemoglobin domain I at 2.2 Å resolution. Molecular features of oxygen avidity. *Proc. Natl. Acad. Sci. USA.* 92:4224–4228.

Zhang, W., F. Cutruzzolà, C. Travaglini-Allocatelli, M. Brunori, and G. N. La Mar. 1997. A myoglobin mutant designed to mimic the oxygen-avid *Ascaris suum* hemoglobin: elucidation of the distal hydrogen bonding network by solution NMR. *Biophys. J.* 73:1019–1030.